RASĀYAN *J. Chem.*
Vol. 19 | No. 3 | 1415-1424 | July-September | 2026
ISSN: 0974-1496 | e-ISSN: 0976-0083 | CODEN: RJCABP
http://www.rasayanjournal.com
http://www.rasayanjournal.co.in

PHYSICOCHEMICAL PROPERTIES AND FUNCTIONAL PERFORMANCE OF CuO-NiO NANOCOMPOSITE FOR ENVIRONMENTAL AND ANTIBACTERIAL APPLICATIONS

R. P. Jakkula[1,2], D. Suresh[1,✉] , S. R. Konda[3], and R. Raghavapuram[1]
[1]Department of Physics and Electronics, Chaitanya (Deemed to be University), Hyderabad-500075, Telangana, India
[2]Science Lab, Department of Physics, Government Polytechnic, Warangal-506007, Telangana, India
[3]Department of Physics, Indian Institute of Technology Ropar, Rupnagar-140001, Punjab, India
✉Correspondence author: suresh.domala@chaitanya.edu.in

ABSTRACT
Pure CuO and CuO–NiO nanocomposite were synthesised via a chemical process. The existence of cubic NiO and monoclinic CuO phases was confirmed by structural analyses. EDS showed the existence of elements Cu, Ni, and O without any discernible impurities; SEM analysis showed nanoscale aggregated morphologies. FTIR spectra showed characteristic Cu–O and Ni–O vibrations, and UV–Vis absorption studies revealed a robust visible-light response with a narrowed band gap upon NiO incorporation. When exposed to visible light, the CuO–NiO composite degraded the methylene blue dye more effectively than pure CuO. The efficient separation of photogenerated electron-hole pairs and effective charge transfer across the interface are all responsible for the enhanced photocatalytic activity of the nanocomposite system. Similarly, the composite system exhibited stronger inhibition against microorganisms due to its components' synergistic interaction and improved surface interface with bacterial cell membranes, which increased oxidative stress and effectively inhibited bacterial growth. The developed composite material can be considered as an integrated system for catalytic and microbial inhibition applications.
Keywords: CuO–NiO Nanocomposite, Hydrothermal Synthesis, Methylene Blue Dye, Photocatalytic Degradation, Antibacterial Activity.
RASĀYAN *J. Chem.*, Vol. 19, No.3, 2026

INTRODUCTION

Due to the rapid advancement of industrialisation and urbanisation, as well as the high pace of global economic development, a lot of environmental challenges have unavoidably emerged recently. As artificial colours are widely used in many different industries, there are serious health and pollution dangers associated with their untreated release into the environment. Methylene blue (MB) dye is a widely used cationic dye in the textile, paper, and pharmaceutical industries and is frequently detected in wastewater.[1] Dyes have been successfully removed from aqueous environments using various treatment methods, such as electrochemical processes, chemical oxidation, adsorption, and photocatalysis.[2-5] Among the various treatment approaches, semiconductor-based photocatalysis is widely regarded as a low-cost, highly efficient, and environmentally benign method. In recent years, the increasing occurrence of antimicrobial resistance has motivated research into advanced antibacterial materials. In view of this, metal oxide-based semiconductors have come to light as potential composite systems for multifunctional performance in treating wastewater and biomedical fields. The composite material design has emerged as a powerful strategy to enhance the functional performance of metal oxides. The integration of multiple phases within a composite system enables tunable physicochemical properties through interfacial interactions, phase distribution, and synergistic effects. Particularly, composite materials are of significant interest in materials science due to their ability to improve charge transfer dynamics and surface reactivity, making them suitable for multifunctional applications. Due to their exceptional chemical and physical characteristics, copper oxide (CuO) and nickel oxide (NiO) have been the subject of extensive research. CuO is a narrow band gap p-type semiconductor (approximately 1.9 eV) with high visible light absorption and fast carrier mobility, whereas NiO is a broad band gap p-type semiconductor

http://doi.org/10.31788/RJC.2026.1939899

(approximately 4 eV) with superior stability, corrosion resistance, and oxidation ability.[6-7] CuO–NiO composites work together to create p–p type junctions that enhance visible light absorption efficiency, reduce electron– hole recombination, and improve interfacial charge transfer.[8-9] CuO–NiO nanocomposites have been investigated for uses in environmental cleanup, gas sensing, water splitting, and supercapacitors.[10-11] Effective charge carrier separation and interfacial band alignment, which increase charge lifetime and produce more reactive sites, are the causes of the increased activity in these composites.[12-13] Most reported studies on CuO-NiO systems have mainly focused on photocatalytic efficiency, whereas studies on antibacterial properties are relatively limited. This work demonstrates the multifunctional nature of the CuO-NiO system synthesised using a cost-effective hydrothermal method, with an emphasis on their structural, morphological, optical, photocatalytic and antibacterial characteristics. The degradation of the methylene blue (MB) dye was used to evaluate the efficiency of the produced samples. Similarly, antibacterial activity was analysed against the positive bacteria, Staphylococcus and the negative bacteria, Pseudomonas. In both cases, the CuO-NiO nanocomposite demonstrated the highest activity. The results highlight CuO–NiO composite as a potential multifunctional agent for efficient environmental cleanup and antibacterial activity.

EXPERIMENTAL

Chemicals

Methylene blue, sodium hydroxide, nickel nitrate hexahydrate, and copper 2,4-pentanedionate were utilised exactly as supplied. Throughout the investigation, deionised water was utilised for all solution preparations, and all compounds were of analytical quality.

Synthesis of Pure CuO and CuO–NiO Nanocomposite

A low-temperature hydrothermal method is used for preparing CuO nanoparticles. A measured quantity of copper 2,4-pentanedionate was dissolved in deionised water under continuous stirring to obtain a homogeneous precursor solution. To attain a stable solution, the pH value was calibrated by NaOH dropwise addition. To ensure complete homogenization after pH adjustment, the reaction mixture was magnetically stirred for an extended period. After that, the mixture was kept in an autoclave with a Teflon seal and heated to 180°C for eight hours in order to encourage hydrothermal crystallisation. Once the precipitate had naturally cooled to room temperature, it was collected, repeatedly cleaned with ethanol and deionised water to eliminate any remaining ions and organic species, then dried to produce pure CuO. The CuO–NiO composite was synthesised using the same hydrothermal process, with the addition of an appropriate nickel precursor along with the copper precursor under identical conditions.

Characterizations

An X-ray diffraction analysis using a Bruker AXS D8 Focus instrument with 20-80 ^{o} Cu Kα radiation (wavelength 1.5406 Å) was used to analyse the crystalline structure of the produced materials. The surface characteristics and elemental distribution of the material was analysed by SEM (ZEISS) integrated with EDX.FTIR was used to identify the functional groups and chemical bonds in the samples. Optical absorption assessments were recorded using a UV-visible spectrophotometer (Hitachi U-4100).

Photocatalytic Test

We used mimic solar light conditions using a 300W xenon lamp as a light source. The irradiation intensity was adjusted to 100 mW/cm^2, while the separation between the source of light and the reactor was kept constant. In a procedure, the prepared photocatalyst was suspended in an aqueous MB dye solution and agitated in the absence of light to establish adsorption–desorption equilibrium. The pH of the suspension can be adjusted using 0.1 M NaOH or dilute acid solutions. After equilibrium, the suspension was exposed to visible light, and samples were collected at regular intervals for analysis. Ten milligrams of MB were dissolved in one thousand millilitres of deionised water to create a stock MB solution (10 mg/L). The reaction suspensions were prepared by introducing the photocatalyst into the dye solution, followed by stirring for half an hour. By continuously exposing to visible light, at 30-minute intervals, 2 mL samples were withdrawn and centrifuged to separate the catalyst particles. The absorbance of the

clear supernatant was then monitored using UV-Visible spectroscopy to track the degradation progress. The photocatalytic degradation efficiency D (%), was computed utilising the subsequent relation.[14]

$$D\ (\%) = \left(1 - \frac{C}{C_0}\right) \times 100 \qquad (1)$$

Here, C_0 is the MB concentration (at initial time t = 0), and C is the MB concentration (at irradiation time t).

Antibacterial Activity

The agar well diffusion method, a widely employed qualitative approach for assessing the antimicrobial efficacy of nanomaterials, was utilised to evaluate the antibacterial properties of the synthesised samples. To make and sterilise nutritional agar medium at 121°C for 15 minutes, standard microbiological methods were used. To ensure uniform bacterial distribution, freshly prepared bacterial suspensions (~10^6 CFU/mL) were uniformly applied on agar plates with sterile cotton swabs after solidification. A predetermined concentration of nanoparticle suspension (50 µL) was carefully added to each well. To be sure that any inhibition noticed was just due to the activity of the nanoparticles, control wells filled with pure water were retained. The plates were kept at 37 °C for 24 hours to make sure that the bacteria and nanoparticles grew and interacted with each other as much as possible. After incubation, a digital calliper was used to measure the diameter of the clear zone of inhibition (ZOI) around each well to see how well the antibacterial worked.

RESULTS AND DISCUSSION

XRD Analysis

The diffraction peaks of both samples exhibit strong and well-defined reflections, confirming their crystalline nature.[15] For the pure CuO sample, the CuO phase's (002), (111), (20-2), and (11-3) planes are represented by separate peaks at 2θ = 35.4°, 38.7°, 48.8°, and 61.4° (JCPDS card no. 48-1548), respectively.[16] The produced CuO nanoparticles' high degree of crystallinity is indicated by the strong and vivid peaks.[17] All characteristic diffraction peaks of CuO remain clearly observable after the incorporation of NiO (Fig.-1(b)), indicating that the fundamental monoclinic structure of CuO is preserved after doping.[18] Nevertheless, the peak intensities exhibit a modest shift toward lower 2θ values and a tiny drop, indicating lattice deformation brought on by interstitial inclusion or Ni^{2+} replacement inside the CuO matrix.[19] Additional faint peaks that appear at 2θ = 37.2° and 43.3° are caused by the (111) plane and (200) plane of the face-centred cubic NiO phase (JCPDS card no. 47-1049).[20] These results verify that the CuO–NiO nanocomposite was successfully formed.[9]

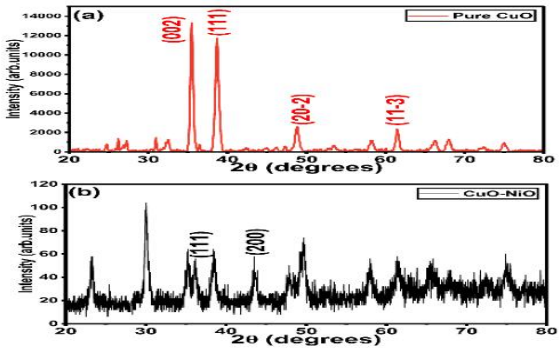

Fig.-1: XRD of the Prepared Samples

EDS Analysis

It shows strong and distinct peaks corresponding to Cu (Kα, Lα) and O (Kα), confirming the formation of copper oxide without detectable impurities.[10,15] In the CuO–NiO nanocomposite, an additional characteristic peak corresponding to Ni is observed along with Cu and O signals, verifying the successful incorporation of NiO into the composite. The values nearly match the anticipated stoichiometry of a CuO-rich CuO–NiO nanostructure. In line with the XRD results, the comparatively lower Ni% indicates that NiO nanoparticles are finely distributed on the CuO surface rather than forming a distinct bulk phase.[18,21] The creation of a well-integrated CuO–NiO composite is supported by the uniform distribution of Cu, Ni,

and O atoms throughout the matrix and is crucial for enhanced charge transfer and interfacial stability.[12] The functional behaviour of CuO–NiO composites can be tuned with the use of such uniform elemental dispersion and defect-controlled Ni inclusion. Recent investigations have revealed similar EDS observations for hydrothermally produced CuO–NiO composites, indicating uniform element distribution and the lack of secondary contaminants, which together enhance photocatalytic and electrochemical performance.[22]

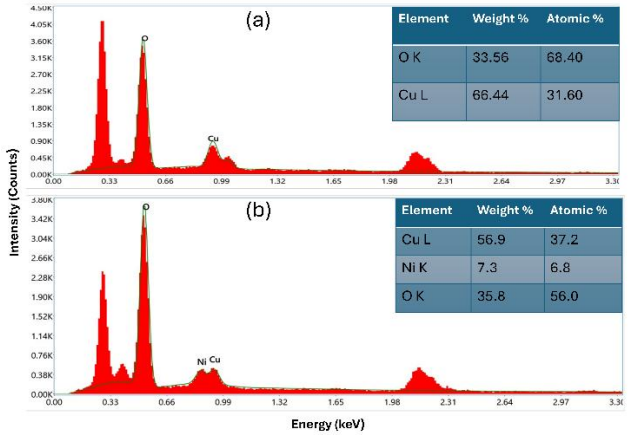

Fig.-2: EDS Spectrum Showing the Elemental Composition

FTIR Analysis

The stretching vibration of O–H groups are due to the absorption band at 3442 cm^{-1} for pure CuO (Fig.-3) and indicates the presence of surface-adsorbed water molecules. The peak at 2915 cm^{-1} is caused by the C–H stretching vibrations. The band at 2335 cm^{-1} that is absorbed from the environment is indicative of the CO_2 stretching vibration. The band at 1614 cm^{-1} is caused by the bending mode of H–O–H. Cu–O stretching vibrations are represented by the peaks at 1043 cm^{-1}, 1386 cm^{-1}, and 621 cm^{-1}, indicating the development of monoclinic CuO.[7,23,24]

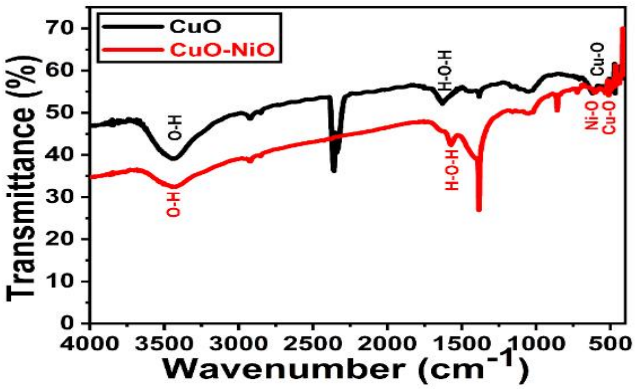

Fig.-3: FTIR Spectra of Prepared Samples

Regarding the CuO–NiO nanocomposite (Fig.-3), the broad band at 3425 cm^{-1} corresponds to O–H stretching vibrations, while the peaks at 2923 cm^{-1}, 2845 cm^{-1}, 2423 cm^{-1}, and 2370 cm^{-1} are due to C–H and CO_2 stretching modes. The absorption band at 1562 cm^{-1} corresponds to H–O–H bending vibrations. The bands appearing at 1386 cm^{-1}, 1158 cm^{-1}, 1035 cm^{-1}, 841 cm^{-1}, 709 cm^{-1}, and 634 cm^{-1} are assigned to metal–oxygen stretching vibrations, indicating the coexistence of Cu–O and Ni–O bonds in the composite structure.[10,22,25] The absence of impurity peaks and the preservation of both Cu–O and Ni–O vibrational modes point to high phase purity and successful composite production. These results, which are in good agreement with XRD and EDS examinations, confirm the formation of a CuO–NiO composite system with stable chemical bonding and minimal surface contamination.[8,9]

SEM Analysis

The SEM image of pure CuO (Fig.-4(a)) shows a compact, rough, and densely packed surface morphology composed of closely spaced nanoparticles. The grains form a continuous network-like structure with no distinct particle boundaries, giving the appearance of being heavily agglomerated. Because of their high surface energy and nanoscale size, the CuO nanoparticles appear to have a strong inclination to cluster, as indicated by their dense aggregation. Overall, the morphology appears fine-grained and relatively homogeneous, suggesting uniform nucleation and growth of CuO crystallites during synthesis.

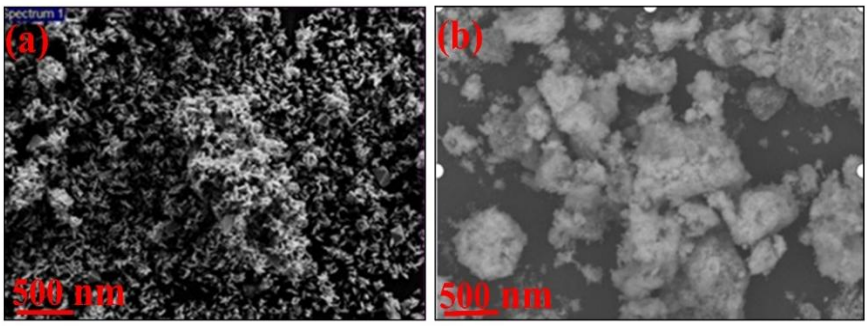

Fig.-4: SEM Images of Prepared Samples

The CuO–NiO nanocomposite (Fig.-4(b)) displays a comparatively coarser surface morphology. There are some discernible porosity areas in between the larger, more erratic, and irregularly scattered particles. This morphological variation suggests that the incorporation of NiO influences the nucleation and growth behaviour of CuO, leading to partial agglomeration and increased surface roughness. As a result, the composite surface displays a rough appearance that is consistent with the formation of a mixed metal-oxide system.[22]

UV-Vis Absorption Spectra and Band Gap Studies

Figure-5 displays the optical absorbance of the generated CuO and CuO-NiO nanocomposite. This discovery revealed that the absorbance peak of CuO was located at about 410 nm. The CuO-NiO nanocomposite surface characteristics resulted in increased light absorption coverage in the visible spectrum, which can be due to interfacial interactions between CuO and NiO. The increased visible light absorption indicates a modification in the electronic structure, which may provide better photocatalytic response.[26]

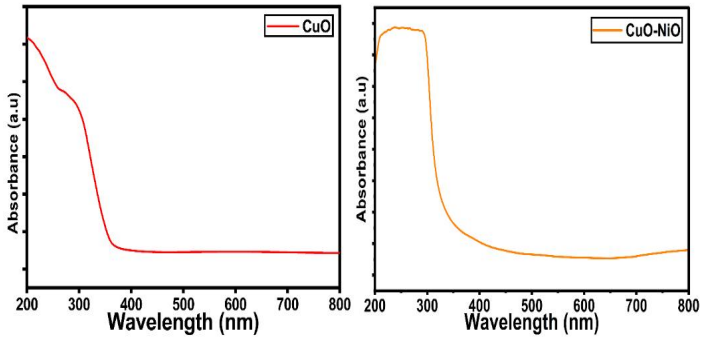

Fig.-5: Absorption Spectra of the Prepared Samples

The bandgap energy calculated using the Tauc relation $(\alpha h\nu)^n = A(h\nu - E_g)$ for a permitted direct transition, n equals 2. The band gap values were estimated to be approximately 2.75 eV for CuO–NiO nanocomposite and 3.02 eV for CuO.[27] The energy gap narrowing in the CuO–NiO composite is caused by a strong electronic interaction between CuO and NiO that encourages charge delocalisation and lowers the energy gap between the valence and conduction bands. The reduced band gap, along with enhanced visible-light absorption, promotes higher photoinduced charge carrier density and prolongs charge carrier lifetime, which is beneficial for the functional performance of the prepared samples. Some recent studies

have reported similar band-gap narrowing in CuO–NiO composites synthesised by hydrothermal or sol–gel techniques, attributing the reduced Eg to effective interfacial charge transfer and defect-induced band alignment.[20,28] Overall, the formation of a CuO–NiO composite significantly enhances the optical properties of the material, making it a promising candidate for visible light photocatalysis.

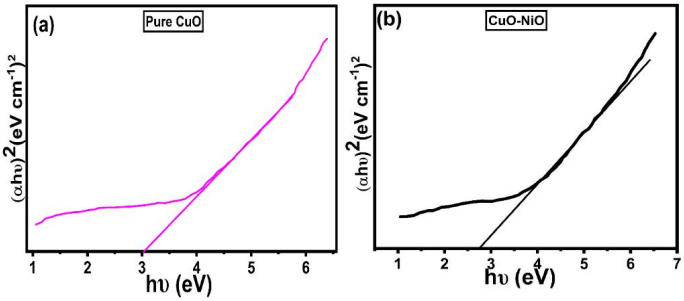

Fig.-6: Tauc Plots for Optical Band Gap Estimation

Photocatalytic Degradation Studies of Methylene Blue Dye

In the case of pure CuO, the characteristic MB absorption peak at λmax = 660 nm decreases slowly with time, indicating limited photocatalytic activity.[29] In contrast, CuO–NiO composite shows a much faster and more pronounced decrease in absorbance intensity at 660 nm with irradiation time. After 180 minutes of exposure to visible light, CuO-NiO exhibited a significantly higher efficiency than pure CuO, demonstrating the superior photocatalytic performance of the composite system (Fig.-7(b)). Control tests under the same irradiation set-up without the photocatalysts confirmed that the dye degradation was primarily due to photocatalytic processes and not caused by light exposure. A first-order kinetic approximation was used to further assess the degradation behaviour and compare the photocatalytic efficiency of the photocatalysts using the equation.[18]

$$\ln\left(\frac{C_0}{C}\right) = kt \qquad (2)$$

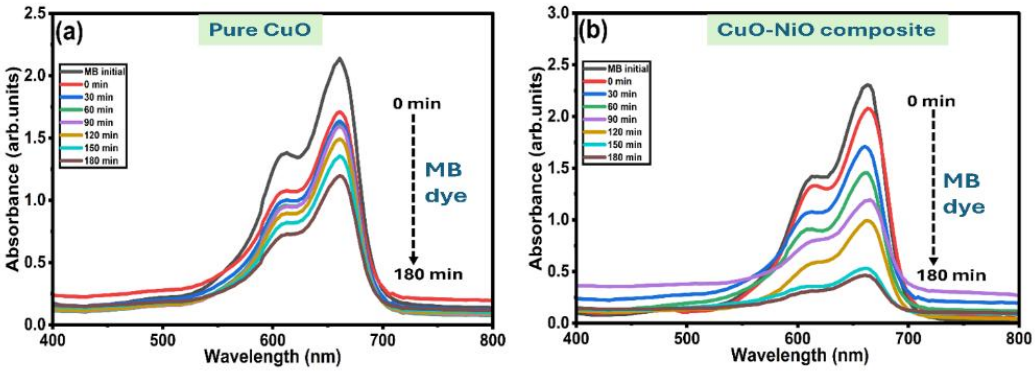

Fig.-7: UV-Vis Absorption Behaviour of MB during Photocatalytic Degradation

It can be observed from the Fig.-8(a) that the decrease in dye concentration was achieved more with composite CuO-NiO, while the straight line trend from Fig.-8(b) gives the rate constants (k) of 0.00183 min^{-1} for CuO and 0.00874 min^{-1} for CuO–NiO, which shows that the composite system with the higher rate constant exhibits faster degradation efficiency compared to the other.

Photocatalytic Degradation Mechanism

By electrostatic attraction and surface interactions, methylene blue dye molecules are adsorbed onto the photocatalyst surface, thereby initiating an adsorption-desorption equilibrium. Fig.-9 illustrates the suggested photocatalytic breakdown pathway of methylene blue dye when exposed to light. An electron is driven from the VB to the CB when the photocatalyst is exposed to light. This leaves behind an electron-deficient, hole (h^+) in the VB.

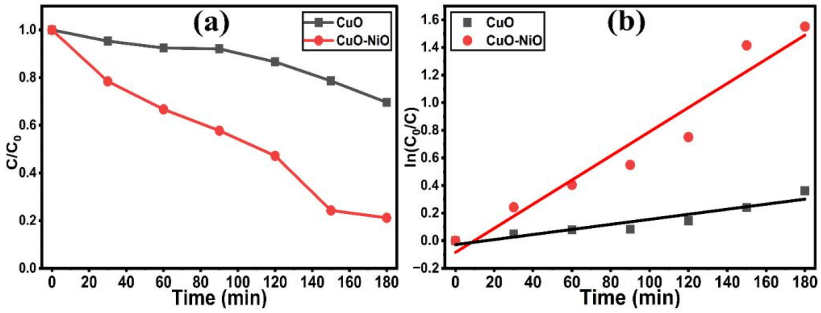

Fig.-8:(a) Normalised Concentration of MB as a Function of Irradiation Time and (b) Linear Kinetic Representation

These electron-hole pairs, which are photogenerated charge carriers, can either undergo recombination or take part in different surface redox processes. Because photogenerated charge carriers quickly recombine, there are fewer electrons and holes available for surface redox processes in pure CuO, which lowers degradation efficiency. In contrast, the CuO-NiO composite effectively suppresses charge-carrier recombination by promoting interfacial charge separation, thereby increasing the lifetime of photogenerated electrons and holes available for surface redox reactions. Upon irradiation, the catalyst generates electron-hole pairs, where holes generate •OH radicals and electrons contribute to O_2^- radicals, which attack dye molecules, and degrade into harmless end products like CO_2 and H_2O.[30]

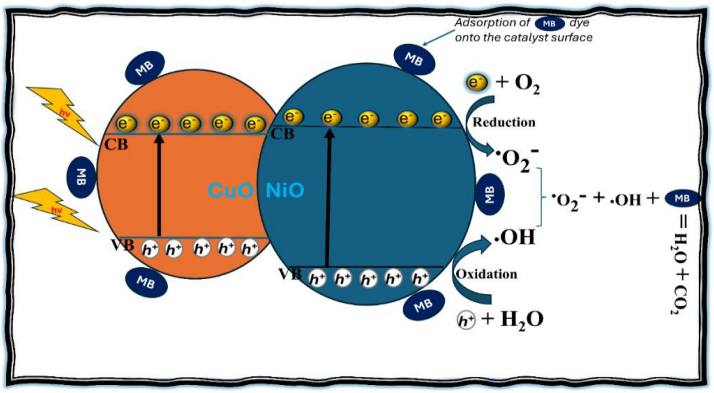

Fig.-9: Possible Reaction Mechanism using CuO–NiO Catalyst

Antibacterial Activity Studies

In our study, the CuO-NiO composite exhibited more antibacterial activity against Gram-positive Staphylococcus bacterium. Both bacterial groups' cell surface amine and carboxyl groups showed a strong attraction for copper ions, resulting in interface interactions. The antibacterial activity of CuO nanostructures may be intimately linked to two oxidation states: cupric (Cu^{2+}) and cuprous (Cu^+). CuO nanostructures produced Cu ions during various oxidation states, which interfered with metabolism, denatured proteins, and inhibited enzyme activity. The manner in which CuO nanostructures' mechanism of growth inhibition involves Cu ion interaction with DNA, which causes cross-linking to harm the molecular structure and strands. CuO nanostructures physically damage bacterial membranes, impairing their permeability and integrity and perhaps leading to cell lysis. Furthermore, CuO nanostructures may interact with biological components or trigger Fenton-like processes to produce reactive oxygen species (ROS). The buildup of ROS in bacteria causes oxidative damage to proteins, lipids, and nucleic acids, thereby interrupting essential cellular functions and metabolic pathways. Moreover, exposure to CuO nanoparticles can reduce bacterial viability by blocking DNA replication and electron transport chain enzyme activity. This mechanism reduces the likelihood of resistance development and worsens bacterial cell death.[31] On incorporating NiO into the CuO matrix, it contributes to collective ROS generation, coupled metal ion toxicity, better charge separation, and preferable interference of bacterial cell membranes, ultimately resulting in CuO-NiO composite exhibiting greater antibacterial performance. The antibacterial activity of the prepared samples is shown in Fig.-10.

Table-1: Diameter of Inhibition

Sample	Staphylococcus	Pseudomonas
Pure CuO	26 mm	18 mm
CuO-NiO composite	32 mm	22 mm

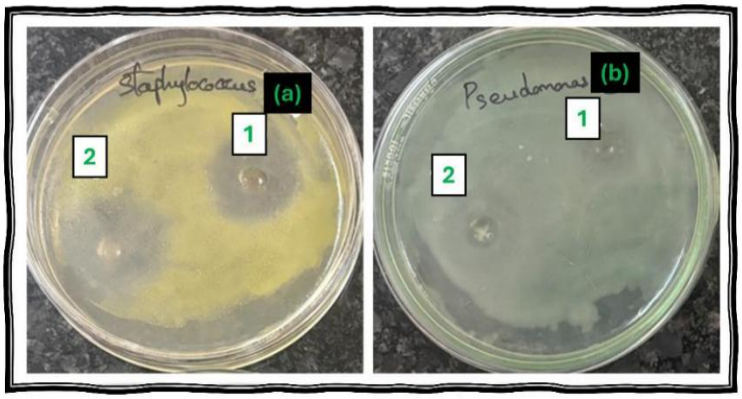

Fig.-10: Antibacterial Performance of CuO(I) and CuO-NiO(2) against (a) Staphylococcus, and (b) Pseudomonas Bacteria

CONCLUSION

The Hydrothermal process is used in the synthesis of pure CuO and CuO-NiO nanocomposite. The nanocrystalline nature of CuO and the presence of CuO and NiO forms in the CuO-NiO composite were confirmed by XRD studies. UV-vis absorption studies revealed a noticeable redshift of the adsorption edge for the CuO–NiO composite compared to pure CuO, suggesting a smaller optical band gap and increased absorption in the visible spectrum. The CuO–NiO composites' efficient migration of electrons and holes, along with better charge mobility, is responsible for the composite's improved photocatalytic activity. Additionally, the increased antibacterial effect of the composite system results from the better generation of reactive oxygen species along with strong interaction with bacterial cell walls. Our studies demonstrated that the prepared composite system can act as a multifunctional agent, highlighting the synergistic role of NiO incorporation into CuO matrix, by improving charge-carrier dynamics, which will play a vital role in photocatalytic and antibacterial applications. These findings emphasise the importance of nanocomposite material design in developing next-generation functional materials for environmental remediation and antimicrobial applications.

CONFLICT OF INTERESTS

The authors declare that there is no conflict of interest.

AUTHOR CONTRIBUTIONS

The present work is related to *SDG-6:Clean Water and Sanitation*. All the authors contributed significantly to this manuscript, participated in reviewing/editing and approved the final draft for publication. The research profile of the authors can be verified from their ORCID ids, given below:

Rajendra Prasad Jakkula https://orcid.org/0009-0002-1759-6149
Domala Suresh https://orcid.org/0000-0002-1673-0054
Srinivasa Rao Konda https://orcid.org/0000-0002-9001-4857
Ramyashree Raghavapuram https://orcid.org/0009-0000-1290-9025

Cite this article as: R. P. Jakkula *et al.*, *Rasayan J. Chem.*, 19(3), 1415-1424(2026), https://doi.org/10.31788/RJC.2026.1939899

REFERENCES

1. P. Oladoye, T. Ajiboye, E. Omotola, and O. Oyewola, *Results in Engineering,* **16**, 100678(2022), https://doi.org/10.1016/j.rineng.2022.100678
2. H. Zhou, H. Wang, C. Yue, L. He, H. Li, H. Zhang, S. Yang, and T. Ma, *Applied Catalysis B: Environment and Energy,* **344**, 123605(2024), https://doi.org/10.1016/J.APCATB.2023.123605
3. H. Berede, D. Andoshe, N. Gultom, D.-H. Kuo, X. Chen, H. Abdullah, T. Wondimu, Y. Wu, and O.A. Zelekew, *Scientific Reports,* **14**, Article 2314(2024), https://doi.org/10.1038/s41598-024-52547-w
4. G. Kosarsoy-Agceli, K. Dulta, P. Chauhan, P. Chauhan, R. Jasrotia, and J. O. Ighalo, *Sustainable Environment Research,* **32**, 2(2022), https://doi.org/10.1186/s42834-021-00111-w
5. M. Singh, P. Kumar, N. S. Singh and A. Jain, *Rasayan Journal of Chemistry,* **16(1)**, 268(2023), http://doi.org/10.31788/RJC.2023.1618076
6. H. Weldekirstos, B. Minlkalewu, and D. Kabtamu, *Frontiers in Materials,* **9**, 1(2022), https://doi.org/10.3389/fmats.2022.832439
7. F. Anjum, M. Shaban, M. Ismail, S. Gul, E. Bakhsh, M. Khan, U. Sharafat, S. Khan, and M. Khan, *ACS Omega*, **8(20)**, 17667(2023), https://doi.org/10.1021/acsomega.3c00129
8. A.L. Lone, S.U. Rehman, S. Haq, A.F. Alkhuriji, N.M. Al-Malahi, J. Razzokov, S. Shujaat, and A. Samad, *RSC Advances,* **15**, 22311 (2025), https://doi.org/10.1039/D5RA02443A
9. K. Dharmalingam, A.K. Bojarajan, R. Gopal, E. Thangavel, S. Omari, and S. Sangaraju, *Scientific Reports*, **14**,14518 (2024), https://doi.org/10.1038/s41598-024-65163-5
10. P. Prabu and V. Losetty, *Inorganic Chemistry Communications*, **169**, 113003(2024), https://doi.org/10.1016/j.inoche.2024.113003
11. K. Kannan, K. Chinnaiah, K. gurushankar Sankar, R. Krishnamoorthi, Y.-S. Chen, P.S.M. Kumar, and L. Yuan-Yao, *Materials,* **17**, 3976 (2024), https://doi.org/10.3390/ma17163976
12. Z. Ishaque, Y. Zaman, A. Arif, A. Siddique, M. Shahzad, D. Ali, M. Aslam, H. Zaman, and M. Faizan Kamboh, *RSC Advances*, **13**, 30838(2023), https://doi.org/10.1039/d3ra05170f
13. N. Morante, K. Monzillo, A. Padua, A. Muscatello, D. Sannino, S. Esposito, and V. Vaiano, *Discover Nano,* **20**, 104 (2025), https://doi.org/10.1186/s11671-025-04296-6
14. N. Gupta, Susmita, and A. Mandavgane, *Rasayan Journal of Chemistry,* **17(4)**, 2033(2024), https://doi.org/10.31788/RJC.2024.1749082
15. M. Uddin, S. Yeasmin, A. Muzahid, M. Rahman, G.M. Rana, T. Chowdhury, M. Al-Amin, M. Wakib, and S. Begum, *Heliyon,* **10**, e30544 (2024), https://doi.org/10.1016/j.heliyon.2024.e30544
16. H.C. Ananda Murthy, T.D. Zeleke, K.B. Tan, S. Ghotekar, M.W. Alam, R. Balachandran, K.Y. Chan, P.F. Sanaulla, M.R. Anil Kumar, and C.R. Ravikumar, *Results in Chemistry*, **3**, 100141(2021), https://doi.org/10.1016/j.rechem.2021.100141
17. A. Ethiraj and D.J. Kang, *Nanoscale Research Letters,* **7**, 70 (2012), https://doi.org/10.1186/1556-276X-7-70
18. A. Elumalai, S. Thanikaikarasan, and E. V Siddhardhan, *Results in Chemistry*, **7**, 101439(2024), https://doi.org/10.1016/j.rechem.2024.101439
19. R. Ganesn, A. Nallathambi, P. Annamalai, G. Sampathkumar, R. Chinnadurai, S. Narayanan, P. Tamizhdurai, R. Kumaran, N. Alsaiari, K. Abualnaja, and M. Ouladsmane, *Journal of Saudi Chemical Society,* **26**, 101440(2022), https://doi.org/10.1016/j.jscs.2022.101440
20. A. Al-Yunus, W. Al-Arjan, H. Traboulsi, and M. Hessien, *International Journal of Molecular Sciences,* **25**, 4119 (2024), https://doi.org/10.3390/ijms25074119
21. T. Tangcharoen, W. Klysubun, and C. Kongmark, *Physica Status Solidi (a)-Applications and Materials Science*, **219(16)**, 2200072(2022), https://doi.org/10.1002/pssa.202200072
22. T.M. Naren Vidaarth, S. Surendhiran, S. Savitha, K.S.G. Jagan, S. Swetha, M. Kathirselvam, R. Mohanraj, and A. Karthik, *Journal of Alloys and Compounds Communications,* **8**, 100121 (2025), https://doi.org/10.1016/J.JACOMC.2025.100121
23. S. Sundar, V. Ganesh, and S. Kwon, *Nanomaterials*, **8**, 823(2018), https://doi.org/10.3390/nano8100823

24. V. Padil and M. Cernik, *International Journal of Nanomedicine*, **8**, 889(2013), https://doi.org/10.2147/IJN.S40599
25. M.W. Alam, M. Aamir, M. Farhan, M. Albuhulayqah, M. Ahmad, R. C. R, D.K. V G, and H.C.A. Murthy, *Crystals,* **11(12)**, 1467(2021), https://doi.org/10.3390/cryst11121467
26. S. Senobari and A. Nezamzadeh-Ejhieh, *Journal of Molecular Liquids*, **261**, 208(2018), https://doi.org/10.1016/j.molliq.2018.04.028
27. X. Zhao, P. Wang, Z. Yan, and N. Ren, *Optical Materials*, **42**, 544(2015), https://doi.org/10.1016/j.optmat.2014.12.032
28. G. Mulatu Mamo and S. Yadeta Ejeta, *Results in Chemistry*, **11**, 101801(2024), https://doi.org/10.1016/J.RECHEM.2024.101801
29. S. Tan, M. Yuen, and R. Ramli, *Green Analytical Chemistry*, **12**, 100230(2025), https://doi.org/10.1016/j.greeac.2025.100230
30. P. Luque, A. Lopez-Peraza, O. Nava, G. Amaya-Parra, Y. Báez, V. Carmona, H. Garrafa-Galvez, and M. Chinchillas-Chinchillas, *Materials*, **14**, 7537 (2021), https://doi.org/10.3390/ma14247537
31. S. Naz, A. Gul, and M. Zia, *IET Nanobiotechnology,* **14**, 1(2019), https://doi.org/10.1049/iet-nbt.2019.0176

[RJC-9899/2026]